Published in final edited form as:
Biochim Biophys Acta Mol Cell Biol Lipids. 2019 April ; 1864(4): 500–511. doi:10.1016/j.bbalip.2019.01.007.

Hepatocyte-specific lysosomal acid lipase deficiency protects mice from diet-induced obesity but promotes hepatic inflammation

Christina Leopold[a], **Madalina Duta-Mare**[a], **Vinay Sachdev**[a], **Madeleine Goeritzer**[a], **Lisa Katharina Maresch**[b], **Dagmar Kolb**[a,c], **Helga Reicher**[a], **Bettina Wagner**[d], **Tatjana Stojakovic**[e], **Thomas Ruelicke**[d], **Guenter Haemmerle**[b], **Gerald Hoefler**[f,g], **Wolfgang Sattler**[a,g], and **Dagmar Kratky**[a,g,*]

[a]Gottfried Schatz Research Center, Medical University of Graz, Graz, Austria

[b]Institute of Molecular Biosciences, University of Graz, Graz, Austria

[c]Center for Medical Research, Medical University of Graz, Graz, Austria

[d]Institute of Laboratory Animal Science, University of Veterinary Medicine Vienna, Vienna, Austria

[e]Clinical Institute of Medical and Chemical Laboratory Diagnostics, Medical University of Graz, Graz, Austria

[f]Diagnostic and Research Institute of Pathology, Medical University of Graz, Graz, Austria

[g]BioTechMed-Graz, Graz, Austria

Abstract

Lysosomal acid lipase (LAL) hydrolyzes cholesteryl esters (CE) and triglycerides (TG) to generate fatty acids (FA) and cholesterol. LAL deficiency (LAL-D) in both humans and mice leads to hepatomegaly, hypercholesterolemia, and shortened life span. Despite its essential role in lysosomal neutral lipid catabolism, the cell type-specific contribution of LAL to disease progression is still elusive. To investigate the role of LAL in the liver in more detail and to exclude the contribution of LAL in macrophages, we generated hepatocyte-specific LAL-deficient mice (*Liv-Lipa*$^{-/-}$) and fed them either chow or high fat/high cholesterol diets (HF/HCD). Comparable to systemic LAL-D, *Liv-Lipa*$^{-/-}$ mice were resistant to diet-induced obesity independent of food intake, movement, and energy expenditure. Reduced body weight gain was mainly due to reduced white adipose tissue depots. Furthermore, *Liv-Lipa*$^{-/-}$ mice exhibited improved glucose clearance

*Corresponding author at: Gottfried Schatz Research Center, Medical University of Graz, Neue Stiftingtalstrasse 6/6, 8010 Graz, Austria. dagmar.kratky@medunigraz.at (D. Kratky).

Transparency document
The Transparency document associated with this article can be found, in online version.

Conflict of interest
The authors declare that there is no conflict of interest associated with this manuscript.

Author contribution
CL and DKr conceived and designed the study and wrote the paper. CL, MDM, VS, MG, LKM, DK, HR, TR, BW, TS, GHae, GHoe, and WS contributed to data collection and analyses. All authors critically revised the manuscript and have read and approved the final version. DKr is responsible for the integrity of the work as a whole.

Europe PMC Funders Author Manuscripts

during glucose and insulin tolerance tests compared to control mice. Analysis of hepatic lipid content revealed a massive reduction of TG, whereas CE concentrations were markedly increased, leading to CE crystal formation in the livers of *Liv-Lipa*$^{-/-}$ mice. Elevated plasma transaminase activities, increased pro-inflammatory cytokines and chemokines as well as hepatic macrophage infiltration indicated liver inflammation. Our data provide evidence that hepatocyte-specific LAL deficiency is sufficient to alter whole-body lipid and energy homeostasis in mice. We conclude that hepatic LAL plays a pivotal role by preventing liver damage and maintaining lipid and energy homeostasis, especially during high lipid availability.

Keywords

LAL-D; Cholesteryl ester storage disease; Wolman disease; Fibrosis; Liver damage; Lipid

1 Introduction

The liver is an essential metabolic organ, and hepatic energy metabolism is tightly controlled by multiple nutrient, hormonal, and neuronal signals, which regulate glucose, lipid, and amino acid metabolism. The liver not only utilizes glucose as metabolic fuel but also converts glucose into fatty acids (FA). After their release from white adipose tissue (WAT) or dietary intake, hepatocytes can take up FA from the circulation. In the fasted state, FA are oxidized mainly in mitochondria to generate energy and ketone bodies [1].

Low-density lipoprotein (LDL) cholesterol and very low-density lipoprotein (VLDL) cholesterol are taken up by hepatocytes *via* receptor-mediated endocytosis and are targeted to the lysosome [2]. Lysosomal acid lipase (LAL) plays a key role in lipid metabolism by the hydrolysis of cholesteryl esters (CE), triglycerides (TG), and retinyl esters in lysosomes [3,4]. To date, LAL is the only known lipase hydrolyzing CE and TG at an acidic pH in mammalian lysosomes [5]. The absence of LAL results in lysosomal accumulation of CE and TG, associated with reduced generation of unesterified FA and cholesterol, which are important molecules for catabolic, anabolic, and signaling pathways [6]. In humans, LAL deficiency (LAL-D) is an autosomal recessive lysosomal storage disorder characterized by mutations in the *Lipa* gene, which causes accumulation of CE and TG in multiple cells and organs [7]. Absence or residual amount of LAL activity determines the severity of the disease, leading to Wolman Disease (WD) or CE storage disease (CESD) [8,9], respectively. While WD patients die within the first year of life [10], CESD is an often underdiagnosed condition [11] with accumulation of CE and TG predominantly in the liver, spleen, gastrointestinal tract, and macrophages [2]. Early death of CESD patients is mainly due to liver failure and/or accelerated atherosclerosis because of chronic hyperlipidaemia [12]. Clinical diagnosis is challenging due to the prevalence (1:40,000 to 1:300,000) [13] and manifestations that overlap with more common lipid-associated disorders like non-alcoholic fatty liver disease (NAFLD) and non-alcoholic steatohepatitis (NASH). In the western civilization, 15–46% of adults suffer from NAFLD [14,15]. The majority of patients exhibit hepatic steatosis in the absence of substantial inflammation or fibrosis [16]. However, 10–30% of patients with NAFLD develop NASH [15], characterized by varying degrees of hepatic inflammation, ballooning of hepatocytes, and fibrosis in addition to liver steatosis.

Europe PMC Funders Author Manuscripts

Reduced LAL activity in adult NAFLD patients [17] indicate a correlation between dysfunctional LAL and fatty liver disease. Recent reports revealed that enzyme replacement therapy with enzymatically active LAL (Sebelipase, Kanuma®) resulted in a reduction of multiple disease-related hepatic and lipid abnormalities in children and adults affected by LAL-D [18,19].

Mice lacking LAL activity resemble human CESD rather than Wolman disease and have been widely used to study the pathophysiological consequences of LAL-D. LAL-deficient (*Lipa*$^{-/-}$) mice are viable with a median life span of approximately one year, but suffer from severe hepatosplenomegaly and progressive loss of WAT [20,21]. *Lipa*$^{-/-}$ mice show reduced circulating leptin concentrations in the fed state, hypercholesterolemia, and hypoglycemia but improved glucose tolerance and insulin sensitivity [4]. The hepatic phenotype is characterized by microvesicular steatosis and infiltration of Kupffer cells forming nests of “fatty lysosomes” [4]. In addition, LAL is critical for maintaining energy homeostasis by shuttling FA derived from circulating lipoproteins to brown adipose tissue during cold exposure [22] and the generation of lipid mediators from peritoneal macrophages [23]. While numerous studies have investigated whole-body LAL-D in mice, the cell type-specific contribution of LAL to disease progression remained elusive. To address the question whether hepatocytes are involved or even responsible for the severe hepatic phenotype of humans and mice suffering from LAL-D, we generated and characterized hepatocyte-specific *Lipa*$^{-/-}$ (*Liv-Lipa*$^{-/-}$) mice.

2 Materials and methods

2.1 Animals and diets

Liv-Lipa$^{-/-}$ mice were generated using a LoxP-Cre approach [24] to allow conditional silencing of LAL specifically in hepatocytes. Briefly, Lipa constitutive knockout first mutant mice carrying the Lipa$^{tm1a(EUCOMM)Hmgu}$/*Biat* on a C57BL/6 N background were generated by the European Conditional Mouse Mutagenesis Program (EUCOMM). The floxed mouse (Lal$^{fl/fl}$) was generated by breeding Lipa$^{tm1a(EUCOMM)Hmgu}$ with FLP deleter mice (Taconic #7089) to create a floxed Lipa^{tm1c} allele with restored Lipa expression. Mice heterozygous for the floxed allele were bred together to obtain homozygous Lipa$^{fl/fl}$ mice that served as controls. Lipa$^{fl/fl}$ mice were then crossed with transgenic mice expressing the Cre recombinase under the control of the albumin promoter (Alb-Cre 003574 Magnuson JAX) to generate tissue-specific Liv-Lipa$^{+/-}$ mice. Mice containing the hepatocyte-specific deletion were then bred homozygously to produce *Liv-Lipa*$^{-/-}$ mice. Animals were housed in groups of 2–4 in filter-top cages (Tecniplast, Hohenpeißenberg, Germany) under standard laboratory conditions on a regular light-dark cycle (12 h/12 h) in a clean and temperature-controlled environment (22 ± 1 °C with relative humidity, 45%–65%). Mice were either fed a regular chow diet (11.9% caloric intake from fat; Altromin Spezialfutter GmbH, Lage, Germany) or challenged with a high-fat/high-cholesterol diet (HF/HCD; 30% caloric intake from fat plus 1% cholesterol; E15741–34 + 1% Cholesterol, Ssniff, Soest, Germany) starting at the age of 7 weeks. Experiments were performed using male and female age- and sex-matched control littermates. Both sexes were used for experiments, as there were no sex-specific differences. *Liv-Lipa*$^{-/-}$ mice had *ad libitum* access to water and food, except when food was restricted

during fasting. Experiments started after 10 weeks on the according diet, or mice were maintained on diets until the end of experiments. The overnight fasting period was 12 to 14 h during the dark cycle. All animal experiments were performed according to the European Directive 2010/63/EU in compliance with national laws and approved by the Austrian Federal Ministry of Education, Science and Research, Vienna, Austria. Experiment licenses were granted under BMWFW-66.010/0109-WF/V/3b/2015.

2.2 Primary mouse hepatocyte isolation and culture

Mice were anesthetized by intraperitoneal injection of 100 μl ketamin (80 mg/kg)/xylazin (12 mg/kg). Primary hepatocytes were isolated by the collagenase perfusion method as described previously [25] and seeded on collagen-coated plates. Parenchymal cells were separated from non-parenchymal cells (NPCs) by centrifugation (50 ×*g*, 3 min, 4 °C). Hepatocytes and NPCs were incubated overnight in M199 medium (Sigma-Aldrich, St. Louis, MO) containing 10% FBS, 23 mM HEPES, 10 nM dexamethasone, 2 mM glutamine, 1% penicillin/streptomycin, 26 mM sodium bicarbonate, and 5.5 mM glucose. The following day, cells were cultivated in FBS-free medium for another 24 h and then used for experiments.

2.3 Lipase activity assays

Livers and hepatocytes from male mice were lysed in lysis buffer (100 mM NaH_2PO_4, pH 6.8, 1 mM EDTA, 10 mM DTT, 0.5% NP-40, 0.02% sodium azid, protease inhibitors) and centrifuged for 10 min at 10,000 ×*g*. LAL activity was estimated at pH 4 using the fluorogenic substrate 4-methyl-umbelliferyl-palmitate as described [26]. Hepatocytes from male mice were lysed in citrate buffer (100 mM citric acid monohydrate, 100 mM trisodium citrate dehydrate, pH 4) and centrifuged at 1000 ×*g* and 4 °C for 10 min. The protein content of the supernatant was determined by a Lowry assay (Bio-Rad, Hercules, USA). Acid TG and CE hydrolase activities using radioactively labeled substrates were measured as previously described [23].

2.4 Reverse transcription and quantitative real-time PCR

Two micrograms of total RNA were reverse transcribed using the High Capacity cDNA Reverse Transcription Kit (Applied Biosystems, Carlsbad, CA). Quantitative real-time PCR was performed on a Roche LightCycler 480 (Roche Diagnostics, Risch, Switzerland) using the QuantiFastTM SYBR® Green PCR Kit (Qiagen, Valencia, CA). Samples were analyzed in duplicate and normalized to the expression of cyclophilin A as reference gene. Expression profiles and associated statistical parameters were determined using the $2^{-\Delta\Delta CT}$ method. Primer pairs are shown in Table S1.

2.5 Western blotting analysis

Hepatocytes were lysed in RIPA buffer and protein concentrations were quantitated (DC™ Protein assay, Bio-Rad Laboratories, Hercules, CA). Hepatocyte lysates (50 μg protein) were separated by SDS-PAGE and transferred onto a PVDF membrane. Non-specific binding sites of the membrane were blocked (5% solution of milk powder or 1% BSA in washing buffer) for 1 h. LAL protein expression was detected using an, anti-rabbit polyclonal antibody

against LAL (1:1000, Origene, Rockville, MD). Polyclonal anti-rabbit calnexin (1:1000; Santa Cruz, Heidelberg, Germany) was used as loading control. HRP-conjugated goat anti-rabbit (1:2500) and rabbit anti-mouse antibodies (1:500; Dako, Glostrup, Denmark) were visualized by enhanced chemiluminescence detection on a ChemiDoc™ MP imaging system (Bio-Rad Laboratories).

2.6 Blood biochemical analyses

Blood was collected by puncture of the v.facialis from *ad libitum* fed or 12 h-fasted mice. TG, TC (DiaSys, Holzheim, Germany), and β-hydroxybutyrate (Cayman, Ann Harbor, MI) concentrations were measured enzymatically according to manufacturer's instructions. Lipoprotein fractions from 200 μl pooled plasma per genotype were separated using fast protein liquid chromatography (Pharmacia P-500) equipped with a Superose 6 column (Amersham Biosciences, Piscataway, NJ) and TG and TC concentrations were assayed spectrophotometrically. Alanine aminotransferase and aspartate aminotransferase levels were measured enzymatically (Roche Diagnostics, Risch, Switzerland). Blood glucose concentration was determined using Accu-Chek® Active glucometer and glucose strips (Roche Diagnostics).

2.7 Glucose tolerance test

Six hour-fasted mice were administered i.p. with 2 g glucose/kg body weight in PBS. Blood glucose levels were measured 0, 15, 30, 60, and 120 min after injection using Accu-Chek® Active glucometer and glucose strips (Roche Diagnostics).

2.8 Insulin tolerance test

Four hour-fasted mice were i.p. injected with 1 IU insulin/kg body weight in PBS (100 IU/ml stock; Actrapid Novo Nordisk, Vienna, Austria). Blood glucose levels were measured 0, 15, 30, 45, 60, and 120 min post-injection using Accu-Chek® Active glucometer and glucose strips (Roche Diagnostics).

2.9 Hepatic lipid concentrations

Liver samples were obtained from female chow diet-fed *Liv-Lipa*$^{-/-}$ and control mice after 12 h of fasting. Hepatic lipid concentrations were measured according to a modified Folch extraction method as described [27].

2.10 FA composition by gas chromatography (GC) analysis

Liver lipids from female HF/HCD-fed mice were extracted twice with chloroform:methanol (2:1, v:v) dried under a stream of nitrogen, and re-dissolved in 1 ml toluol. Aliquots were separated by thin layer chromatography under argon using hexane:diethylether:acetic acid (70:30:1; v:v:v) as mobile phase. Plates were dried, standards were stained with iodine vapor, and phospholipid (PL), diacylglycerol (DG), FA-, TG-, and CE-corresponding bands were scraped off the plates. After addition of the internal standard (pentadecanoic acid), lipids were transesterified (1.2 ml toluene and 1 ml boron trifluoride-methanol (20%)) directly on the silica gel at 110 °C for 1 h. GC analysis of the corresponding FA methyl

esters was performed as described [28] and composition was quantitated by peak area comparison with the internal standard and normalized to protein concentrations.

2.11 Electron microscopy

Liver morphology was assessed in 12 h-fasted female control and *Liv-Lipa*$^{-/-}$ mice challenged with a HF/HCD for 10 weeks. The livers were fixed in phosphate buffer/2.5% glutaraldehyde for 2 h, washed, post-fixed in phosphate buffer/OsO_4 for 2 h and 4 × 10 min in phosphate buffer. After dehydration, tissues were infiltrated (acetone and agar 100 epoxy resin, pure agar 100 epoxy resin) for 4 h, placed in agar 100 epoxy resin (8 h), transferred into embedding molds, and polymerized (48 h, 60 °C). Sections stained with lead citrate and platinum blue were imaged at 120 kV with a Tecnai G 2 FEI microscope (FEI, Eindhoven, Netherlands) equipped with a Gatan ultrascan 1000 CCD camera. Cytosolic lipid droplets (LDs) from 97 electron micrographs (each having a surface of 142.09 μm^2) per genotype were counted and analyzed by open source ImageJ software image processing and analysis in Java.

2.12 Histochemistry and immunohistochemistry

Tissues of male HF/HCD-fed control and *Liv-Lipa*$^{-/-}$ mice were fixed in 4% neutral-buffered formaldehyde for 24 h and embedded in paraffin. Sections (5 μm) were de-paraffinized and subjected to chromotrope aniline blue (CAB) and hematoxylin and eosin (HE) staining, respectively, using standard histopathological techniques [29]. For macrophage staining, sections were incubated with anti-mouse F4/80 antibody (1:50; Serotec MCA 497GA; Biorad, Hercules, CA). Antibody binding was visualized using aminoethyl carbazole substrate chromogen (cat#3464; Dako, Glostrup, Denmark). For neutral lipid staining, 7 μm cryosections were stained with Oil Red O (ORO) and nuclei were counter-stained with Mayer's hematoxylin.

2.13 Statistics

Statistical analyses were performed using GraphPad Prism 5.0 software (GraphPad Software Inc., San Diego, CA). Significances were determined by Student's unpaired *t*-test and Welch correction (in case of unequal variances) for two group comparison and ANOVA followed by Bonferroni correction for multiple group comparison. Data are presented as mean values ± SD. Significance levels were set at $p < 0.05$ (*), $p \leq 0.01$ (**), and $p \leq 0.001$ (***).

3 Results

3.1 Efficient loss of LAL activity in *Liv-Lipa*$^{-/-}$ mice

Defective lysosomal lipolysis in global *Lipa*$^{-/-}$ mice with hepatomegaly, microvesicular steatosis and infiltration of Kupffer cells leading to formation of “fatty lysosomes” [4] rendered global *Lipa*$^{-/-}$ mice impossible to study the contribution of hepatocytes to the severe liver phenotype. We used the FRT-FLP and Cre-loxP system to disrupt a 600 bp region of the *Lipa* gene (Fig. S1). Crossing of mice carrying the floxed *Lipa* allele (*Lipa*$^{fl/fl}$) with mice expressing the Cre recombinase under control of the albumin promoter [30] resulted in hepatocyte-specific *Lipa*-deficient (*Liv-Lipa*$^{-/-}$) mice. *Liv-Lipa*$^{-/-}$ mice are viable and born at Mendelian frequency and proportional male/female ratios (data not

shown). *Lipa* mRNA expression in livers of *Liv-Lipa*$^{-/-}$ mice were reduced by 93% compared to controls, but remained unchanged in other tissues (Fig. 1A). In hepatocytes, *Lipa* mRNA expression and LAL activity were reduced by 99% and 70%, respectively, in *Liv-Lipa*$^{-/-}$ mice compared to controls (Fig. 1B, C). The selectivity of LAL deletion exclusively in hepatocytes was verified as LAL activity in non-parenchymal cells of *Liv-Lipa*$^{-/-}$ and control mice was identical, while it was reduced by 70% in hepatocytes (Fig. 1D). The non-parallel decrement between *Lipa* mRNA expression and LAL activity prompted us to determine LAL protein expression in isolated hepatocytes, which revealed complete absence of LAL in *Liv-Lipa*$^{-/-}$ hepatocytes (Fig. 1E). By providing specific substrates for TG and CE hydrolysis at an acidic pH, we found a 70% reduction in TG hydrolase activity (Fig. 1F) and an even more pronounced reduction (90%) of CE hydrolase activity (Fig. 1G) in *Liv-Lipa*$^{-/-}$ compared to control hepatocytes.

3.2 Increased hepatic cholesterol concentrations in chow diet-fed *Liv-Lipa*$^{-/-}$ mice

We analyzed the impact of hepatocyte-specific LAL deficiency on whole-body energy homeostasis by indirect calorimetry. *Liv-Lipa*$^{-/-}$ mice fed a regular chow diet exhibited a higher respiratory exchange ratio (Fig. S2A), suggestive of enhanced reliance on the breakdown and oxidation of carbohydrates for ATP generation (Fig. S2B) and reduced lipid oxidation (Fig. S2C), while energy expenditure remained unchanged (Fig. S2D). This result was attributed to the fact that food intake (Fig. S2E) and physical activity were comparable in *Liv-Lipa*$^{-/-}$ and control mice (Fig. S2F). Despite unchanged body (Fig. 2A) and liver weight (Fig. 2B, C), we found an 8-fold increase of hepatic CE concentrations in 12 h-fasted *Liv-Lipa*$^{-/-}$ mice (Fig. 2D), in accordance with increased neutral lipid staining (Fig. 2E). As CE accumulation is a characteristic hallmark of both CESD and Wolman disease [7], these findings emphasize the suitability of this mouse model to study the direct consequences of diminished LAL activity in hepatocytes.

3.3 HF/HCD-fed *Liv-Lipa*$^{-/-}$ mice are resistant to diet-induced obesity

The increase in hepatic cholesterol concentrations on a regular chow diet containing only 4% fat encouraged us to investigate *Liv-Lipa*$^{-/-}$ mice after HF/HCD feeding. Already after 8 weeks on diet, *Liv-Lipa*$^{-/-}$ mice weighed up to 8 g (35% of body weight) less than their control littermates (Fig. 3A, B). Despite unaltered food intake (Fig. S3A), movement (Fig. S3B), energy expenditure (Fig. S3C), and fecal energy content (Fig. S3D), *Liv-Lipa*$^{-/-}$ mice had 68% reduced perigonadal WAT weight after 20 weeks of feeding (Fig. 3C). Since *Liv-Lipa*$^{-/-}$ mice have smaller WAT depots, we analyzed WAT and brown adipose tissue (BAT) morphology by H&E staining. We observed comparable white and brown adipocyte size and cell appearance between genotypes (Fig. 3D), indicating rather reduced white adipocyte number in *Liv-Lipa*$^{-/-}$ mice. In analogy to *Lipa*$^{-/-}$ mice [4], we expected plasma lipid parameters in the fasted state to be affected by hepatocyte-specific LAL deficiency. While *Liv-Lipa*$^{-/-}$ mice exhibited comparable plasma TG, we found increased TC concentrations in comparison to control mice (Fig. 3E). Plasma lipoprotein profiles after separation by fast protein liquid chromatography revealed increased LDL but unchanged HDL cholesterol (Fig. 3F). Collectively, these findings indicate that hepatocyte-specific loss of LAL leads to global metabolic changes in *Liv-Lipa*$^{-/-}$ mice.

3.4 Improved glucose clearance in HF/HCD-fed *Liv-Lipa*$^{-/-}$ mice

Hepatic accumulation of lipids, reduced fat mass, and higher reliance on carbohydrate (Fig. S3E) than lipid metabolism (Fig. S3F) led us further investigate glucose metabolism-related changes. While glucose tolerance as well as insulin sensitivity were not altered in chow diet-fed *Liv-Lipa*$^{-/-}$ mice (Fig. S4A, B), we observed improved glucose clearance after HF/HCD feeding (Fig. 4A). Moreover, *Liv-Lipa*$^{-/-}$ mice displayed a significant drop and delay in the normalization of blood glucose levels after an insulin challenge (Fig. 4B), indicating increased insulin sensitivity. We therefore assessed mRNA expression of genes involved in gluconeogenesis and found a significant reduction in *Pcx* (pyruvate carboxylase, 34%), *Mdh* (malate dehydrogenase, 32%), *Pepck* (phosphoenolpyruvate carboxykinase, 59%), and *G6pase* (glucose-6-phosphatase, 64%) expression (Fig. 4C). In line, mRNA levels of the tricarboxylic acid cycle *Cs* (citrate synthase), *Suclg2* (succinate-Coenzyme A ligase), *Fh* (fumarate hydratase), and *Pdhb* (pyruvate dehydrogenase) were reduced (41%, 44%, 23%, and 35%, respectively) (Fig. 4D). Interestingly, β-hydroxybutyrate concentrations were increased in plasma of HF/HCD-fed *Liv-Lipa*$^{-/-}$ mice (Fig. 4E), indicating enhanced formation of ketone bodies for energy supply.

3.5 Increased liver size and CE crystal formation in HF/HCD-fed *Liv-Lipa*$^{-/-}$ mice

Liv-Lipa$^{-/-}$ mice have enlarged and discolored livers (Fig. 5A). The abundance of hepatic cytosolic LDs and the overall lipid load was reduced (Fig. 5B), whereas total liver mass (Fig. 5C) as well as liver mass relative to body weight (Fig. S5A) were significantly increased in *Liv-Lipa*$^{-/-}$ mice. Comparable to our findings in global *Lipa*$^{-/-}$ mice [4], ultrastructural analysis by electron microscopy confirmed that the majority of lipid present in *Liv-Lipa*$^{-/-}$ livers accumulate inside lysosomes with only few cytosolic LDs, while controls accumulate solely cytosolic LDs. Comparable neutral TG hydrolase activity (data not shown) argues against a compensatory increase of neutral TG hydrolases. Furthermore, we observed CE crystals in the cytoplasm of *Liv-Lipa*$^{-/-}$ hepatocytes (Fig. 5D). Detailed size distribution analysis of the LDs proved that predominantly small LDs are present in the livers of *Liv-Lipa*$^{-/-}$ mice (Fig. 5E) resulting in a reduced total LD area (Fig. 5F). Whereas lipid accumulation in intestine and kidney as well as splenomegaly are observed in whole-body *Lipa*$^{-/-}$ mice [21], *Liv-Lipa*$^{-/-}$ mice fed a HF/HCD for 10 weeks showed unaltered weight or morphology in these tissues (Fig. S5B–E). Our findings clearly demonstrate that hepatocyte-specific LAL deletion leads to lysosomal neutral lipid accumulation and CE crystal formation exclusively in the liver.

3.6 Accumulation of fatty acid species mainly in the CE fraction of HF/HCD-fed *Liv-Lipa*$^{-/-}$ mice

To analyze the lipid accumulation in more detail, we determined the PL and neutral lipid composition of *Liv-Lipa*$^{-/-}$ livers by GC analysis. We found a 6.9-fold increase in CE concentrations in livers of HF/HCD-fed *Liv-Lipa*$^{-/-}$ mice. DG and TG concentrations were reduced by 40% and 62%, respectively, whereas other lipid species were unaffected (Fig. 6A). Analysis of the relative distribution of the respective lipid classes revealed increased FA levels in the CE fraction and a decrease in the TG fraction (Fig. S6A). Despite unchanged total hepatic FA concentrations (Fig. 6A), 16:1 and 20:4 FA were reduced in *Liv-Lipa*$^{-/-}$

mice (Fig. 6B). FA composition of PL was comparable between the genotypes (Fig. 6C). In DG and TG fractions, the unsaturated FA species 16:1, 18:1, 18:2, 20:4, and 22:6 were significantly reduced by > 50% (Fig. 6D, E). Despite a substantial decrease in hepatic TG concentrations in *Liv-Lipa*$^{-/-}$ mice, VLDL secretion after inhibition of peripheral lipolysis by tyloxapol was unchanged (Fig. S6B). In contrast, all FA species in the CE fraction were increased with qualitatively most pronounced changes in 18:0, 18:1, 18:2, 20:4, and 22:6 (Fig. 6F). These findings indicate that liver lipid accumulations are due to the incomplete CE hydrolysis in *Liv-Lipa*$^{-/-}$ mice.

3.7 Increased hepatic inflammation in HF/HCD-fed *Liv-Lipa*$^{-/-}$ mice

Increased CE concentrations as well as hepatic CE crystal formation are critically involved in liver inflammation and hepatic steatosis [31]. We therefore performed chromotrope aniline blue staining, which showed increased collagen content indicating liver fibrosis in HF/HCD-fed *Liv-Lipa*$^{-/-}$ mice. Immunohistochemical analysis using the macrophage marker F4/80 revealed a drastically increased number of positive cells compared to control mice. In contrast to global *Lipa*$^{-/-}$ mice [4], the Kupffer cells in *Liv-Lipa*$^{-/-}$ mice are lipid-free (Fig. 7A). mRNA expression of *Ckt19* (cytokeratin 19), *Mcsf* (macrophage colony stimulating factor), *Tgfb* (transforming growth factor beta), and *Col3a* (collagen type III alpha 1 chain) were significantly upregulated, indicating liver injury, inflammation, and fibrosis (Fig. 7B). Accordingly, plasma concentrations of the liver damage markers aspartate aminotransferase and alanine aminotransferase were increased by 11- and 28-fold, respectively (Fig. 7C). Together with the upregulation of various chemokines and cytokines (Fig. 7D), these data suggest that deficiency of LAL in hepatocytes is associated with liver inflammation and incipient fibrosis as a response to HF/HCD feeding.

4 Discussion

The current study demonstrates the physiological importance of hepatocyte-specific LAL activity in whole body energy and lipid homeostasis. Our data provide strong evidence that ablation of LAL in hepatocytes is responsible for the phenotype observed in *Lipa*$^{-/-}$ mice with regard to hepatic CE accumulation, inflammation, and fibrosis. The 8-fold increase in hepatic cholesterol levels in *Liv-Lipa*$^{-/-}$ is in line with previous studies of global *Lipa*$^{-/-}$ mice [4,20,21]. However, body weights of chow diet-fed *Liv-Lipa*$^{-/-}$ and control mice were comparable due to similar food intake, energy expenditure, and physical activity between the genotypes. An increase in carbohydrate oxidation and a decrease in lipid oxidation suggest that *Liv-Lipa*$^{-/-}$ mice rely on carbohydrates for ATP production. When challenged with HF/HCD, *Liv-Lipa*$^{-/-}$ mice were resistant to diet-induced obesity with reduced body weight gain starting already after 8 weeks of feeding despite unaltered food intake, movement, energy expenditure, and fecal energy content. We therefore speculate that energy derived from the diet is not stored in WAT to the same extent as in control mice, but is immediately used for metabolic pathways. After 20 weeks of HF/HCD feeding, *Liv-Lipa*$^{-/-}$ mice showed a 68% reduction in perigonadal WAT weight, being (at least in part) responsible for the reduced body weight. While both the resting metabolic ratio and the activity-related energy expenditure account for total energy expenditure, small changes in either of them markedly

impact total energy expenditure [32]. However, a correlation between body weight and physical activity was absent in *Liv-Lipa*$^{-/-}$ mice.

Since *Liv-Lipa*$^{-/-}$ mice, similar to *Lipa*$^{-/-}$ mice [4,21,22], have reduced WAT depots, we also expected plasma lipid parameters to be altered. Indeed, we found increased cholesterol concentrations in plasma of HF/HCD-fed *Liv-Lipa*$^{-/-}$ mice. Hypercholesterolemia is a hallmark in patients suffering from LAL-D and to date statin treatments brought little benefit in ameliorating dyslipidemia [2,12]. While both LAL-D patients as well as global *Lipa*$^{-/-}$ mice [2,4,12] show decreased HDL cholesterol levels, *Liv-Lipa*$^{-/-}$ mice showed unchanged HDL cholesterol but increased LDL cholesterol concentrations in plasma. Despite increased intra-hepatic cholesterol concentrations and circulating LDL cholesterol concentrations, mRNA expression levels of the downstream effectors of FXR/LXR/SREBP2 (*e.g. HmgCoAr*, *Abcg5/g8*, *Ldlr*) were unchanged (data not shown).

Increased carbohydrate oxidation and highly improved glucose clearance after a glucose tolerance test suggest extensive glucose utilization for energy production in *Liv-Lipa*$^{-/-}$ mice (comparable with global *Lipa*$^{-/-}$ mice). Markedly decreased mRNA expression of genes involved in gluconeogenesis (including *Pepck* and *G6Pase*) and the tricarboxylic acid cycle argue for impaired gluconeogenesis (and possibly glycogenolysis) in HF/HCD-fed *Liv-Lipa*$^{-/-}$ mice. Impaired gluconeogenesis is a driver of ketogenesis and higher plasma levels of β-hydroxybutyrate indicate a shift toward ketone body formation for energy supply. In fact, chronic treatment with butyrate keeps mice metabolically normal on a high-fat diet [33]. Butyrate treatment is further associated with lower glucose and insulin levels, higher glucose tolerance, reduced weight gain, and improved respiratory efficiency [33]. Hepatocytes oxidize FA to generate ketone bodies or incorporate TG into VLDL particles. Ketone bodies and VLDL are secreted from the liver and utilized by extrahepatic tissues. The increase in β-hydroxybutyrate secretion and the unaltered VLDL secretion in *Liv-Lipa*$^{-/-}$ mice guarantee the availability of substrates for extra-hepatic tissues and might explain comparable adipocyte sizes in WAT and BAT of *Liv-Lipa*$^{-/-}$ and control mice. Since other tissues are only affected in global *Lipa*$^{-/-}$ mice [20,21], we conclude that the observed effects are exclusively the consequences of LAL deficiency in hepatocytes.

LAL-D leads especially to CE (and TG) accumulation in hepatocytes and liver-resident macrophages (Kupffer cells) with subsequent progression to fibrosis. The prevalence of liver fibrosis with development of cirrhosis in LAL-D suggests that the accumulation of lysosomal CE and TG is a potent driver of liver fibrosis [2,34–36]. Similar to global *Lipa*$^{-/-}$ mice [4,7,20], we observed enlarged livers with CE crystal formation and accumulation of lipids mainly in lysosomes of *Liv-Lipa*$^{-/-}$ mice. Significantly reduced FA concentrations in the DG and TG fraction might explain the reduced total LD area in livers of *Liv-Lipa*$^{-/-}$ mice. CE crystal formation activates Kupffer cells, leading to inflammation and liver damage [31]. Previous studies using whole-body *Lipa*$^{-/-}$ mice provided evidence for a significant role of LAL in the regulation of inflammation-relevant functions in various tissues [4,21,37]. LAL-D in humans and mice causes a severe phenotype with elevated transaminase activities, which are well established indicators of liver damage. Increased pro-inflammatory cytokines and the massive abundance of macrophages in various organs, predominantly in lung, intestine, liver, and spleen, suggest systemic inflammation [21]. Increased plasma

transaminases in *Liv-Lipa*$^{-/-}$ mice as well as upregulation of hepatic cytokines and chemokines, known to drive inflammation and leading to Kupffer cell activation and liver damage, indicate that LAL in hepatocytes plays a critical role in maintaining liver homeostasis and function. In accordance with our data, expression of human LAL in hepatocytes of *Lipa*$^{-/-}$ mice corrected liver inflammation [38], whereas LAL expression in myeloid cells mainly ameliorated lysosomal lipid accumulation in Kupffer cells with minor effects in other liver cells and the small intestine [37].

Until now, it has been speculated that macrophages trigger lipid accumulation in various tissues of global *Lipa*$^{-/-}$ mice and are responsible for the pathology of LAL-D. From our study, we conclude that macrophages infiltrate the liver as a consequence of impaired hepatocyte LAL activity to clear dietary lipids. Our data provide evidence that the pathology of LAL-D (at least in mice) is mainly driven by hepatocytes, leading to an alteration in hepatic energy homeostasis and resistance to diet-induced obesity. Consequently, CE accumulation induces Kupffer cell activation, causing inflammation and liver damage in HF/HCD-fed *Liv-Lipa*$^{-/-}$ mice.

Supplementary Material

Refer to Web version on PubMed Central for supplementary material.

Acknowledgements

The authors thank S. Rainer, A. Ibovnik, L. Frank, S. Schauer, and D. Pernitsch (Medical University of Graz, Austria) as well as Lill Andersen and Tina Bernthaler (University of Veterinary Medicine Vienna, Austria) for excellent technical assistance, A. Absenger and I. Hindler (Medical University of Graz, Austria) for mice care, and Werner De Cecco (University of Graz, Austria) for technical support with the fecal energy content measurements.

Financial support

This work was supported by the FWF Austrian Science Fund (DK-MCD W1226, P27070, P30882), the BioTechMed-Graz-funded flagship project “Lipases and Lipid Signaling”, the INFRAFRONTIER-i3 #312325 (WP8) project, and the PhD program “Molecular Medicine” at the Medical University of Graz.

Abbreviations

LAL	lysosomal acid lipase
CE	cholesteryl ester
TG	triglycerides
FA	fatty acids
LAL-D	LAL deficiency
HF/HCD	high fat/high cholesterol diet
LDL	low-density lipoprotein
VLDL	very low-density lipoprotein
CESD	CE storage disease

Europe PMC Funders Author Manuscripts

NAFLD	non-alcoholic fatty liver disease
NASH	non-alcoholic steatohepatitis
WAT	white adipose tissue
NPCs	non-parenchymal cells
GC	gas chromatography
PL	phospholipid
DG	diacylglycerol
LD	lipid droplet
HE	hematoxylin and eosin staining
Pcx	pyruvate carboxylase
Mdh	malate dehydrogenase
Pepck	phosphoenolpyruvate carboxykinase
G6pase	glucose-6-phosphatase
Cs	citrate synthase
Suclg2	succinate-Coenzyme A ligase
Fh	fumarate hydratase
Pdhb	pyruvate dehydrogenase
Ckt19	cytokeratin 19
Mcsf	macrophage colony stimulating factor
Tgfb	transforming growth factor beta
Col3a	collagen type III alpha 1 chain

References

[1]. Rui L. Energy metabolism in the liver. Compr Physiol. 2014; 4:177–197. DOI: 10.1002/cphy.c130024 [PubMed: 24692138]

[2]. Bernstein DL, Hulkova H, Bialer MG, Desnick RJ. Cholesteryl ester storage disease: review of the findings in 135 reported patients with an underdiagnosed disease. J Hepatol. 2013; 58:1230–1243. DOI: 10.1016/j.jhep.2013.02.014 [PubMed: 23485521]

[3]. Grumet L, Eichmann TO, Taschler U, Zierler KA, Leopold C, Moustafa T, et al. Lysosomal acid lipase hydrolyzes retinyl ester and affects retinoid turnover. J Biol Chem. 2016; 291:17977–17987. DOI: 10.1074/jbc.M116.724054 [PubMed: 27354281]

[4]. Radovic B, Vujic N, Leopold C, Schlager S, Goeritzer M, Patankar JV, et al. Lysosomal acid lipase regulates VLDL synthesis and insulin sensitivity in mice. Diabetologia. 2016; 59:1743–1752. DOI: 10.1007/s00125-016-3968-6 [PubMed: 27153842]

[5]. Sheriff S, Du H, Grabowski GA. Characterization of lysosomal acid lipase by site-directed mutagenesis and heterologous expression. J Biol Chem. 1995; 270:27766–27772. [PubMed: 7499245]

[6]. Zechner R, Madeo F, Kratky D. Cytosolic lipolysis and lipophagy: two sides of the same coin. Nat Rev Mol Cell Biol. 2017; 18:671–684. DOI: 10.1038/nrm.2017.76 [PubMed: 28852221]

[7]. Grabowski DA, Du H, Charnas L. Lysosomal Acid Lipase Deficiencies: The Wolman Disease/ Cholesteryl Ester Storage Disease Spectrum. The Online Metabolic and Molecular Bases of Inherited Disease. 2002; doi: 10.1036/ommbid.172

[8]. Anderson RA, Rao N, Byrum RS, Rothschild CB, Bowden DW, Hayworth R, et al. In situ localization of the genetic locus encoding the lysosomal acid lipase/cholesteryl esterase (LIPA) deficient in Wolman disease to chromosome 10q23.2-q23.3. Genomics. 1993; 15:245–247. DOI: 10.1006/geno.1993.1052 [PubMed: 8432549]

[9]. Sloan HR, Fredrickson DS. Enzyme deficiency in cholesteryl ester storage idisease. J Clin Invest. 1972; 51:1923–1926. DOI: 10.1172/JCI106997 [PubMed: 5032533]

[10]. Patrick AD, Lake BD. Deficiency of an acid lipase in Wolman's disease. Nature. 1969; 222:1067–1068. [PubMed: 5787090]

[11]. Aguisanda F, Thorne N, Zheng W. Targeting Wolman disease and cholesteryl ester storage disease: disease pathogenesis and therapeutic development. Curr Chem Genom Transl Med. 2017; 11:1–18. DOI: 10.2174/2213988501711010001 [PubMed: 28401034]

[12]. Valayannopoulos V, Mengel E, Brassier A, Grabowski G. Lysosomal acid lipase deficiency: Expanding differential diagnosis. Mol Genet Metab. 2017; 120:62–66. DOI: 10.1016/j.ymgme.2016.11.002 [PubMed: 27876313]

[13]. Scott SA, Liu B, Nazarenko I, Martis S, Kozlitina J, Yang Y, et al. Frequency of the cholesteryl ester storage disease common LIPA E8SJM mutation (c.894G > A) in various racial and ethnic groups. Hepatology. 2013; 58:958–965. DOI: 10.1002/hep.26327 [PubMed: 23424026]

[14]. Browning JD, Szczepaniak LS, Dobbins R, Nuremberg P, Horton JD, Cohen JC, et al. Prevalence of hepatic steatosis in an urban population in the United States: impact of ethnicity. Hepatology. 2004; 40:1387–1395. DOI: 10.1002/hep.20466 [PubMed: 15565570]

[15]. Williams CD, Stengel J, Asike MI, Torres DM, Shaw J, Contreras M, et al. Prevalence of nonalcoholic fatty liver disease and nonalcoholic steatohepatitis among a largely middle-aged population utilizing ultrasound and liver biopsy: a prospective study. Gastroenterology. 2011; 140:124–131. DOI: 10.1053/j.gastro.2010.09.038 [PubMed: 20858492]

[16]. Matteoni CA, Younossi ZM, Gramlich T, Boparai N, Liu YC, McCullough AJ. Nonalcoholic fatty liver disease: a spectrum of clinical and pathological severity. Gastroenterology. 1999; 116:1413–1419. [PubMed: 10348825]

[17]. Baratta F, Pastori D, Del Ben M, Polimeni L, Labbadia G, Di Santo S, et al. Reduced lysosomal acid lipase activity in adult patients with non-alcoholic fatty liver disease. EBioMedicine. 2015; 2:750–754. DOI: 10.1016/j.ebiom.2015.05.018 [PubMed: 26288848]

[18]. Burton BK, Balwani M, Feillet F, Baric I, Burrow TA, Camarena Grande C, et al. A phase 3 trial of Sebelipase alfa in lysosomal acid lipase deficiency. N Engl J Med. 2015; 373:1010–1020. DOI: 10.1056/NEJMoa1501365 [PubMed: 26352813]

[19]. Rader DJ. Lysosomal acid lipase deficiency–a new therapy for a genetic lipid disease. N Engl J Med. 2015; 373:1071–1073. DOI: 10.1056/NEJMe1509055 [PubMed: 26352819]

[20]. Du H, Duanmu M, Witte D, Grabowski GA. Targeted disruption of the mouse lysosomal acid lipase gene: long-term survival with massive cholesteryl ester and triglyceride storage. Hum Mol Genet. 1998; 7:1347–1354. [PubMed: 9700186]

[21]. Du H, Heur M, Duanmu M, Grabowski GA, Hui DY, Witte DP, et al. Lysosomal acid lipase-deficient mice: depletion of white and brown fat, severe hepatosplenomegaly, and shortened life span. J Lipid Res. 2001; 42:489–500. [PubMed: 11290820]

[22]. Duta-Mare M, Sachdev V, Leopold C, Kolb D, Vujic N, Korbelius M, et al. Lysosomal acid lipase regulates fatty acid channeling in brown adipose tissue to maintain thermogenesis. Biochim Biophys Acta. 2018; 1863:467–478. DOI: 10.1016/j.bbalip.2018.01.011

[23]. Schlager S, Vujic N, Korbelius M, Duta-Mare M, Dorow J, Leopold C, et al. Lysosomal lipid hydrolysis provides substrates for lipid mediator synthesis in murine macrophages. Oncotarget. 2017; 8:40037–40051. DOI: 10.18632/oncotarget.16673 [PubMed: 28402950]

[24]. Kos CH. Cre/loxP system for generating tissue-specific knockout mouse models. Nutr Rev. 2004; 62:243–246. [PubMed: 15291397]

[25]. Stoeckman AK, Towle HC. The role of SREBP-1c in nutritional regulation of lipogenic enzyme gene expression. J Biol Chem. 2002; 277:27029–27035. DOI: 10.1074/jbc.M202638200 [PubMed: 12016216]

[26]. Cortner JA, Coates PM, Swoboda E, Schnatz JD. Genetic variation of lysosomal acid lipase. Pediatr Res. 1976; 10:927–932. DOI: 10.1203/00006450-197611000-00005 [PubMed: 10546]

[27]. Obrowsky S, Chandak PG, Patankar JV, Povoden S, Schlager S, Kershaw EE, et al. Adipose triglyceride lipase is a TG hydrolase of the small intestine and regulates intestinal PPARalpha signaling. J Lipid Res. 2013; 54:425–435. DOI: 10.1194/jlr.M031716 [PubMed: 23220585]

[28]. Sattler W, Puhl H, Hayn M, Kostner GM, Esterbauer H. Determination of fatty acids in the main lipoprotein classes by capillary gas chromatography: BF3/methanol transesterification of lyophilized samples instead of Folch extraction gives higher yields. Anal Biochem. 1991; 198:184–190. [PubMed: 1838668]

[29]. Titford M. The long history of hematoxylin. Biotech Histochem. 2005; 80:73–78. DOI: 10.1080/10520290500138372 [PubMed: 16195172]

[30]. Postic C, Shiota M, Niswender KD, Jetton TL, Chen Y, Moates JM, et al. Dual roles for glucokinase in glucose homeostasis as determined by liver and pancreatic beta cell-specific gene knock-outs using Cre recombinase. J Biol Chem. 1999; 274:305–315. [PubMed: 9867845]

[31]. Ioannou GN, Haigh WG, Thorning D, Savard C. Hepatic cholesterol crystals and crown-like structures distinguish NASH from simple steatosis. J Lipid Res. 2013; 54:1326–1334. DOI: 10.1194/jlr.M034876 [PubMed: 23417738]

[32]. Van Klinken JB, van den Berg SA, Havekes LM, Willems Van Dijk K. Estimation of activity related energy expenditure and resting metabolic rate in freely moving mice from indirect calorimetry data. PLoS One. 2012; 7doi: 10.1371/journal.pone.0036162

[33]. Gao Z, Yin J, Zhang J, Ward RE, Martin RJ, Lefevre M, et al. Butyrate improves insulin sensitivity and increases energy expenditure in mice. Diabetes. 2009; 58:1509–1517. DOI: 10.2337/db08-1637 [PubMed: 19366864]

[34]. Marshall WC, Ockenden BG, Fosbrooke AS, Cumings JN. Wolman's disease. A rare lipidosis with adrenal calcification. Arch Dis Child. 1969; 44:331–341. [PubMed: 5785183]

[35]. Konno T, Fujii M, Watanuki T, Koizumi K. Wolman's disease: the first case in Japan. Tohoku J Exp Med. 1966; 90:375–389. [PubMed: 5972796]

[36]. Crocker AC, Vawter GF, Neuhauser EB, Rosowsky A. Wolman's disease: three new patients with a recently described lipidosis. Pediatrics. 1965; 35:627–640. [PubMed: 14269714]

[37]. Yan C, Lian X, Li Y, Dai Y, White A, Qin Y, et al. Macrophage-specific expression of human lysosomal acid lipase corrects inflammation and pathogenic phenotypes in lal−/− mice. Am J Pathol. 2006; 169:916–926. DOI: 10.2353/ajpath.2006.051327 [PubMed: 16936266]

[38]. Du H, Zhao T, Ding X, Yan C. Hepatocyte-specific expression of human lysosome acid lipase corrects liver inflammation and tumor metastasis in lal(−/−) mice. Am J Pathol. 2015; 185:2379–2389. DOI: 10.1016/j.ajpath.2015.05.021 [PubMed: 26212911]

Europe PMC Funders Author Manuscripts

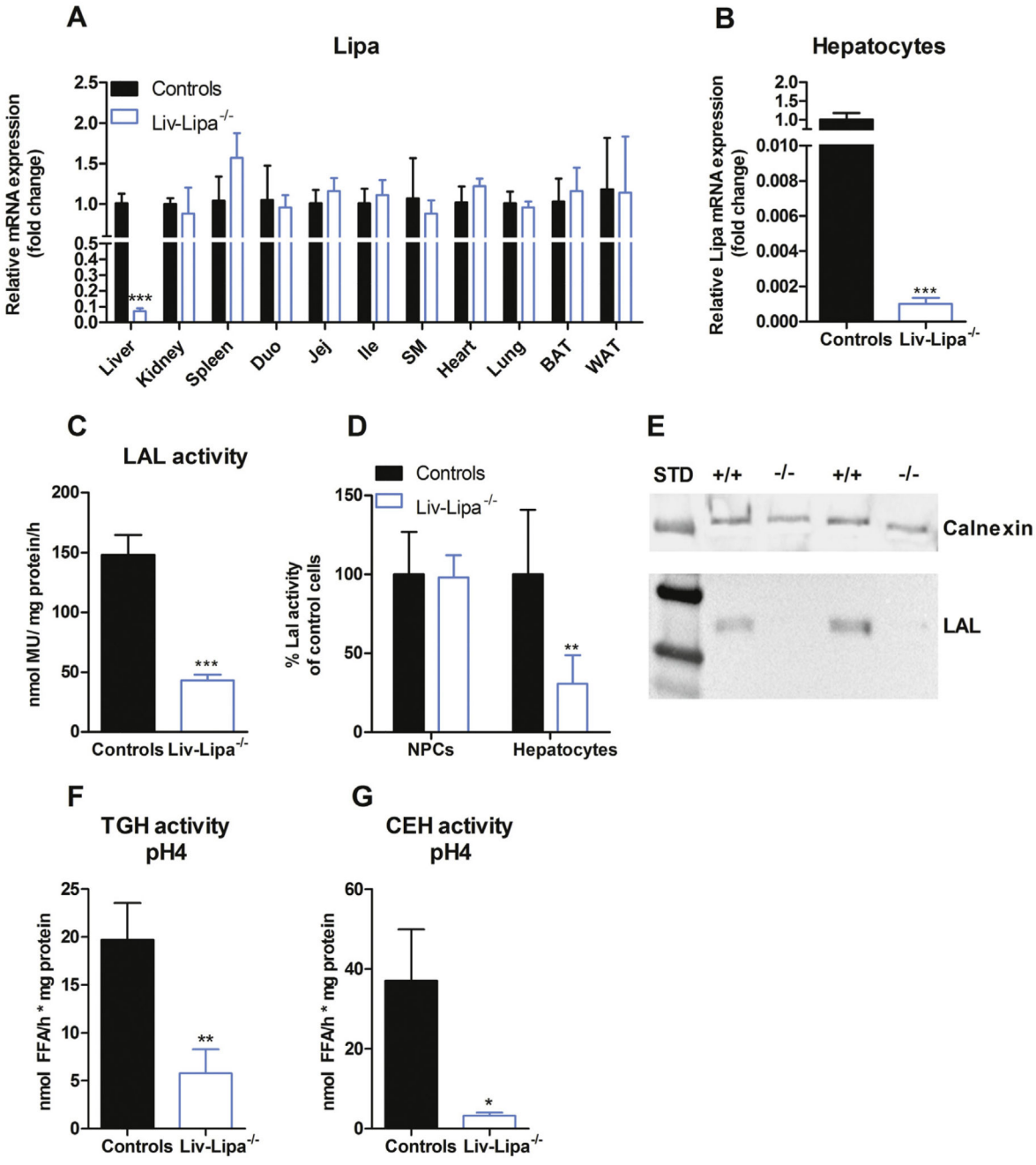

Fig. 1.

LAL is efficiently knocked out in hepatocytes of *Liv-Lipa*$^{-/-}$ mice. Fifteen week old male *ad libitum* chow diet-fed Lipa$^{fl/fl}$ (controls) and *Liv-Lipa*$^{-/-}$ mice were used. Lipa mRNA expression relative to cyclophilin A as reference gene in (A) indicated tissues (n = 4) and (B) hepatocytes (n = 3) (Duo, Duodenum; Jej, Jejunum; Ile, Ileum; SM, skeletal muscle; BAT, brown adipose tissue; WAT, white adipose tissue). Expression profiles were determined using the $2^{-\Delta\Delta CT}$ method and *Lipa* mRNA expression in control mice was arbitrarily set to 1. LAL activity in (C) livers (n = 4–6), (D) non-parenchymal cells (NPCs) (n = 3), and

hepatocytes was determined using a fluorogenic substrate at pH 4 (n = 5). (E) Immunoblotting against LAL using calnexin as loading control. (F) TG hydrolase activity (pH 4) and (G) CE hydrolase activity (pH 4) in hepatocytes (n = 3). Data represent mean + SD; $p < 0.05$ (*), $p \leq 0.01$ (**), $p \leq 0.001$ (***). (A–F) Student's unpaired *t*-test.

Europe PMC Funders Author Manuscripts

Europe PMC Funders Author Manuscripts

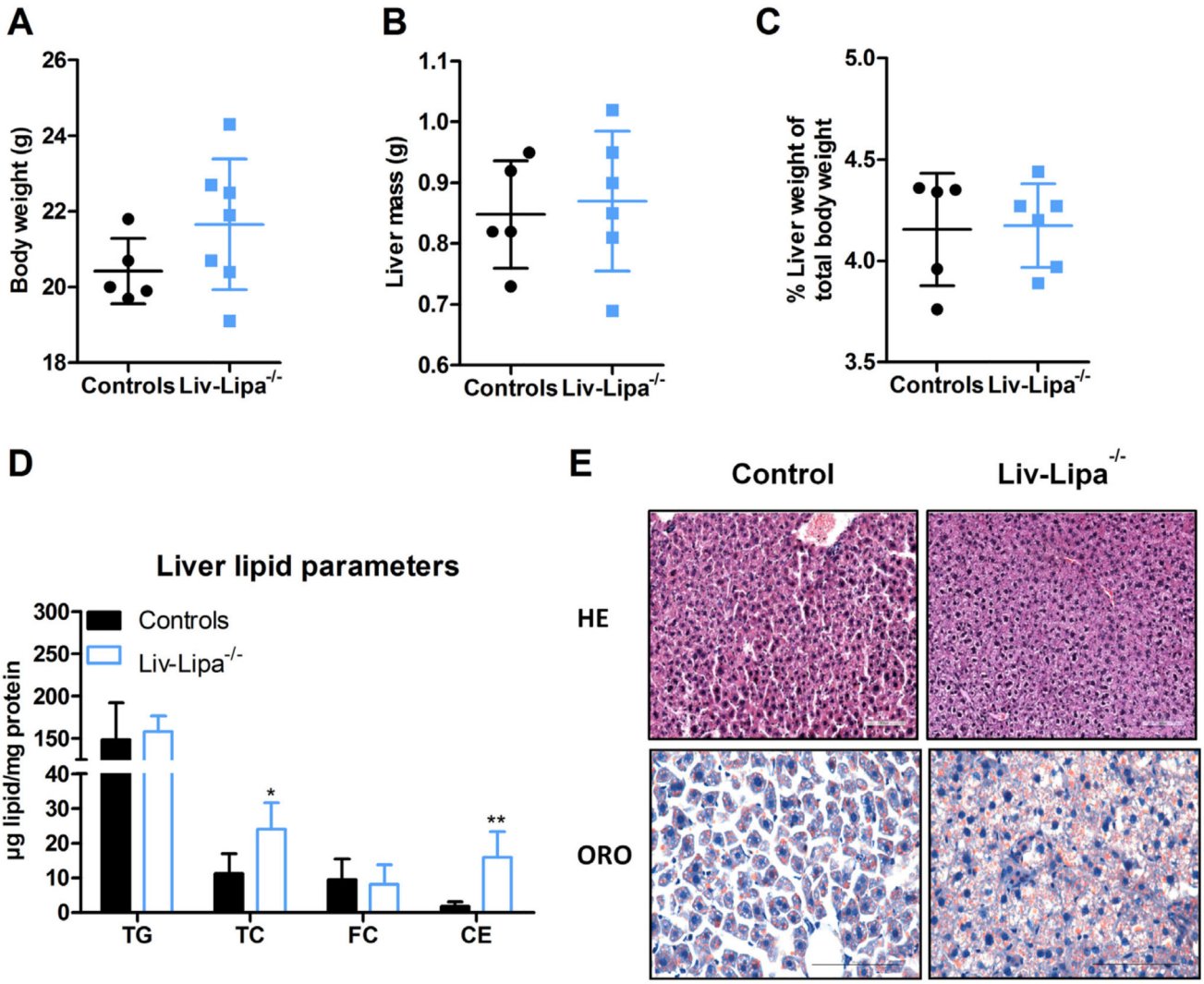

Fig. 2.

Increased hepatic cholesterol concentrations in chow diet-fed *Liv-Lipa*$^{-/-}$ mice. (A) Body weight, (B) total liver weight, and (C) liver weight relative to body weight of 20 week old female chow diet-fed control and *Liv-Lipa*$^{-/-}$ mice. (D) Hepatic lipid parameters. (E) HE staining (upper panel) and Oil red O (ORO) staining (lower panel) of liver sections (scale bar, 100 µm). Data represent mean (n = 5–7) ± SD; $p < 0.05$ (*), $p \leq 0.01$ (**). (A–D) Student's unpaired *t*-test.

Europe PMC Funders Author Manuscripts

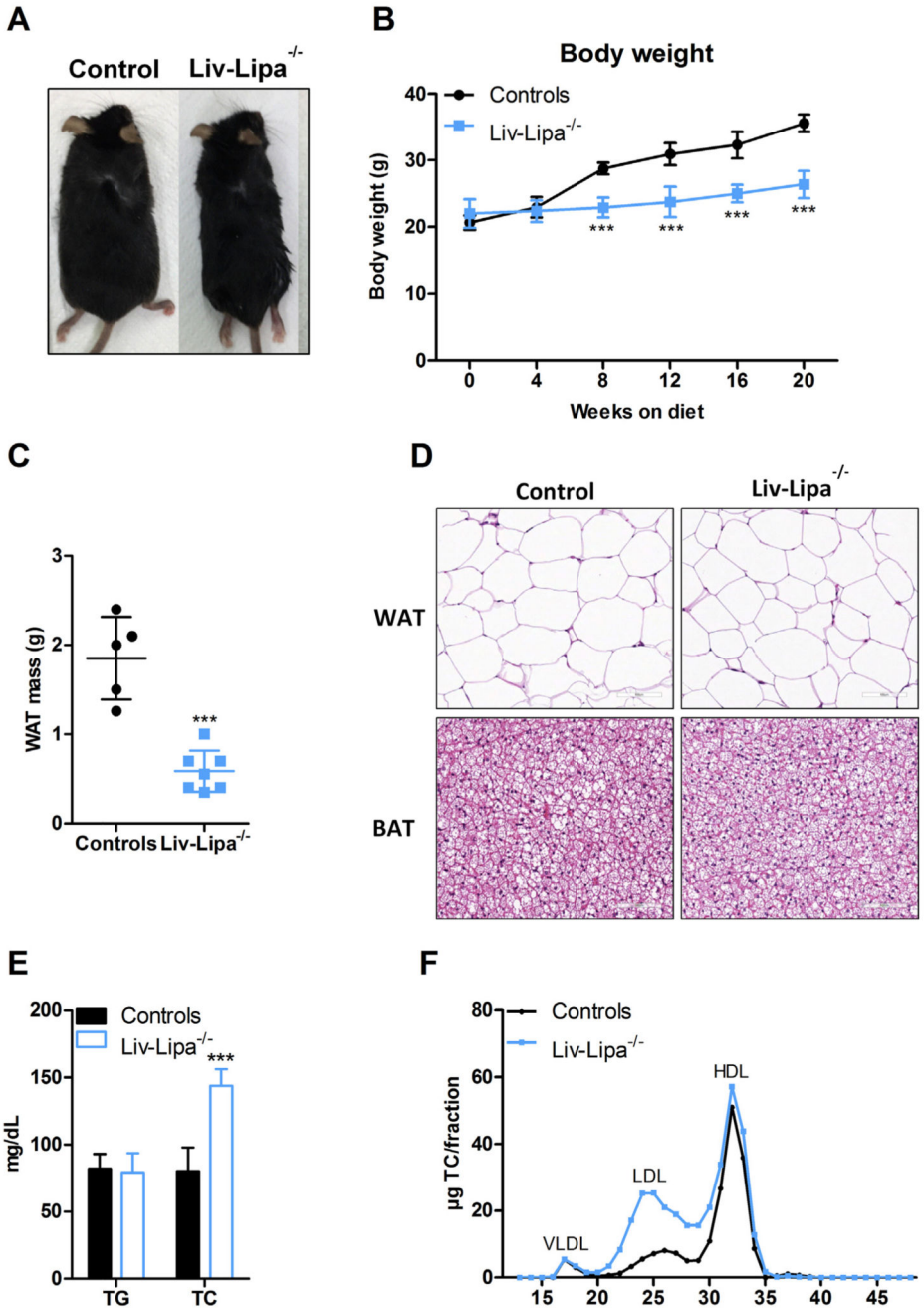

Fig. 3.

Liv-Lipa$^{-/-}$ mice are resistant to diet-induced obesity. (A) Representative image of a male control and a *Liv-Lipa*$^{-/-}$ mouse fed HF/HCD for 10 weeks. (B) Body weight curves and (C) perigonadal WAT weights of female control and *Liv-Lipa*$^{-/-}$ mice after 20 weeks on HF/HCD. (D) H&E staining of WAT and brown adipose tissue sections of male HF/HCD-fed *Liv-Lipa*$^{-/-}$ and control mice (scale bar, 100 µm). (E) Plasma triglyceride (TG) and total cholesterol (TC) concentrations in 12 h-fasted female mice. (F) Lipoprotein profile of pooled plasma samples after fast protein liquid chromatography separation in female mice (n

= 8). Data represent mean ± SD; $p \leq 0.001$ (***). (B) ANOVA. (C, E) Student's unpaired *t*-test.

Europe PMC Funders Author Manuscripts

Europe PMC Funders Author Manuscripts

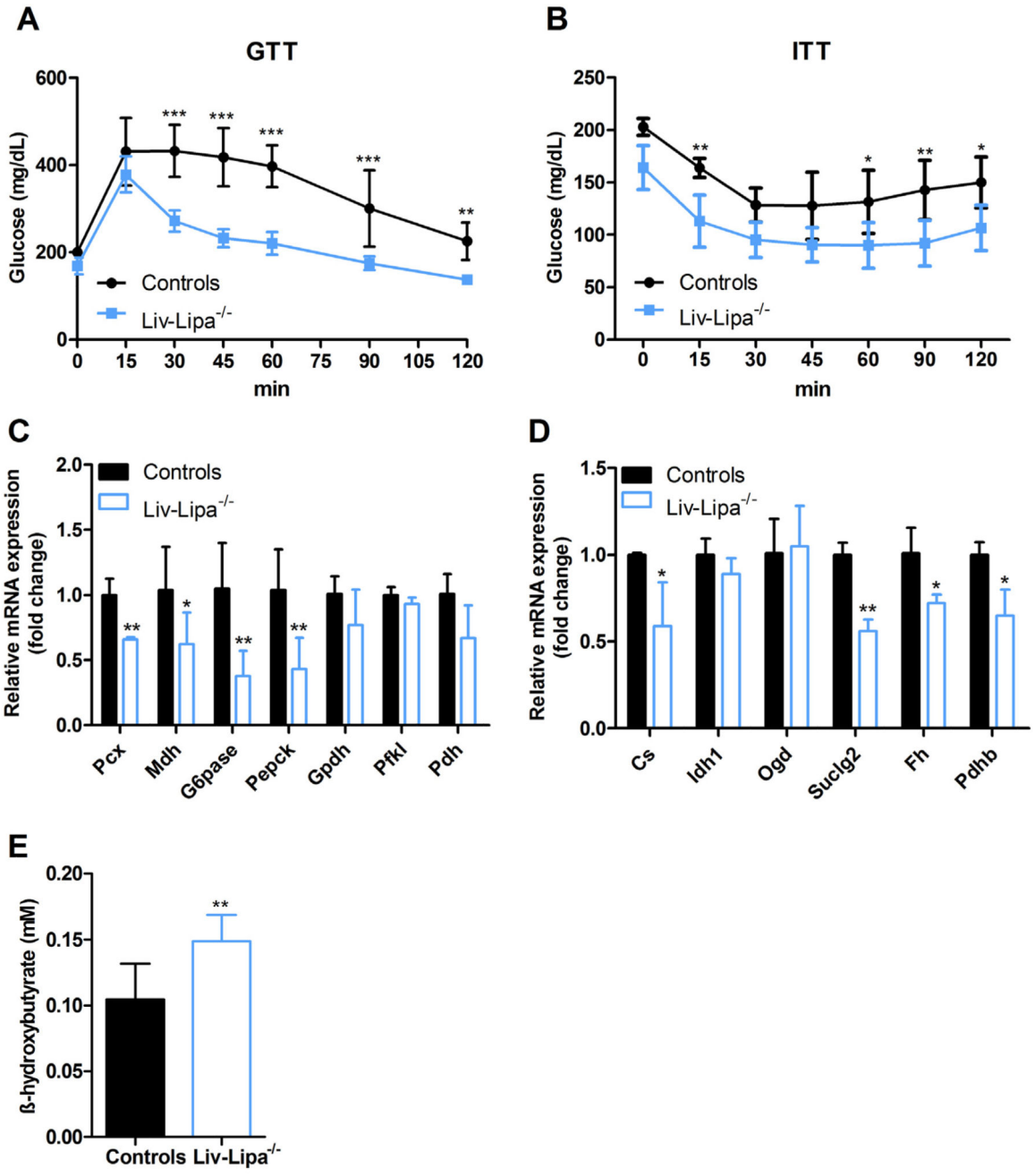

Fig. 4.

Improved glucose clearance in HD/HCD-fed *Liv-Lipa*$^{-/-}$ mice. GTT and ITT were performed in female control and *Liv-Lipa*$^{-/-}$ mice fed HFHCD for 10 and 12 weeks, respectively. Plasma glucose concentrations after i.p. injection of (A) glucose (2 g/kg) and (B) insulin (0.25 U/kg), respectively (n = 8). Hepatic mRNA expression of genes involved in (C) gluconeogenesis and (D) tricarboxylic acid cycle genes relative to cyclophilin A as reference gene in female mice fed a HF/HCD for 20 weeks (n = 3–7). (E) Plasma β-hydroxybuyrate concentrations in male mice fed HF/HCD for 10 weeks (n = 5–7). Data

represent mean ± SD; $p < 0.05$ (*), $p \leq 0.01$ (**), $p \leq 0.001$ (***). (A, B) ANOVA. (C–E) Student's unpaired *t*-test.

Europe PMC Funders Author Manuscripts

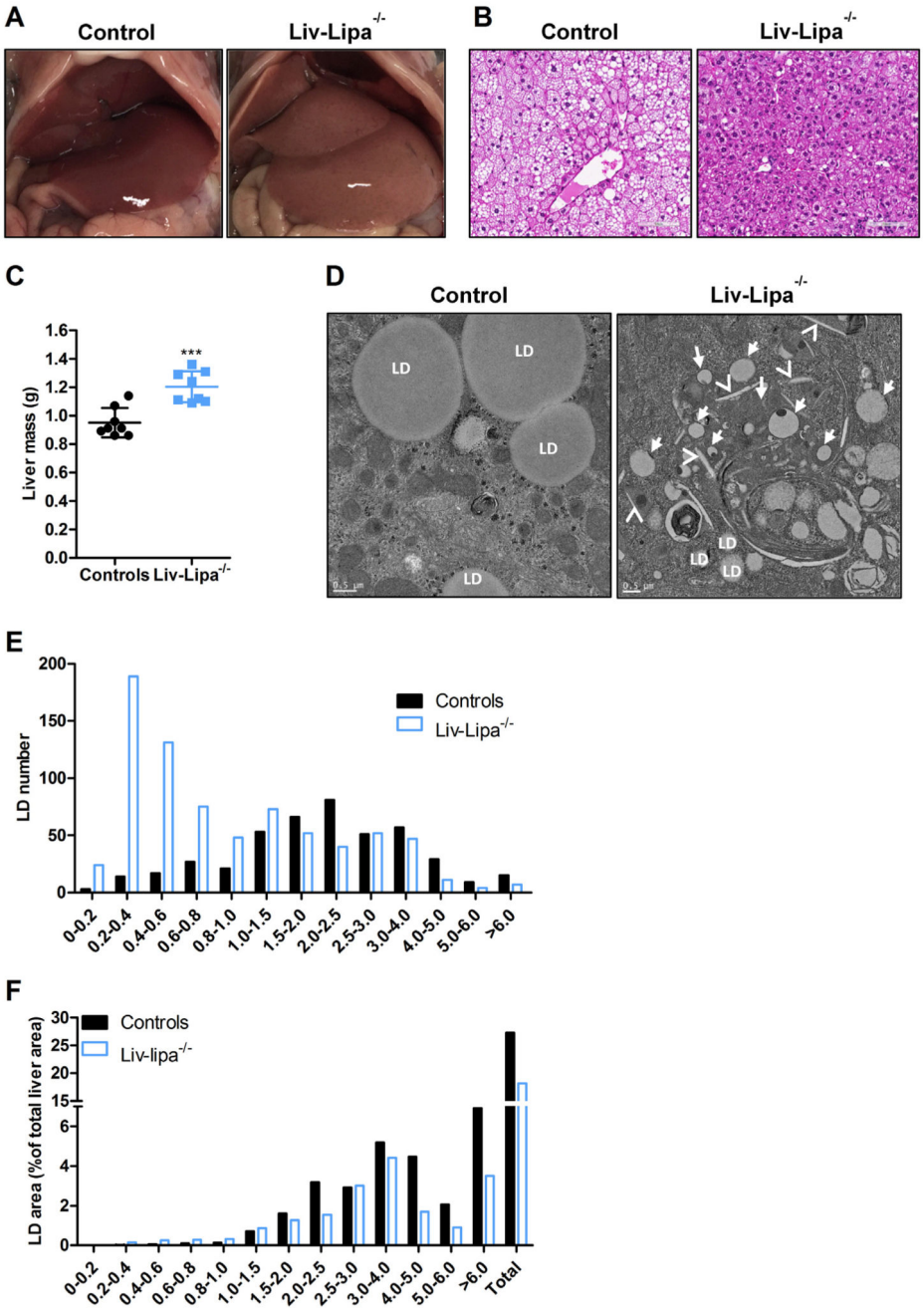

Fig. 5.

Increased liver size and CE crystal formation in HF/HCD-fed *Liv-Lipa*$^{-/-}$ mice. (A) Representative images of livers and (B) representative HE staining of liver sections (scale bar, 100 μm) from male control and *Liv-Lipa*$^{-/-}$ mice fed HF/HCD for 10 weeks. (C) Total liver weight (n = 8) and (D) representative electron micrographs of livers (scale bar 0,5 μm) from mice fed HF/HCD for 10 weeks; LD indicates cytosolic lipid droplets, arrows indicate lipid-laden lysosomes, arrow heads indicate CE crystals. (E) LD distribution and (F) % of

LD area calculated from 60 electron micrographs (each 142.09 μm^2) per genotype. Data represent mean ± SD; $p \leq 0.001$ (***). (B) Student's unpaired *t*-test.

Europe PMC Funders Author Manuscripts

Europe PMC Funders Author Manuscripts

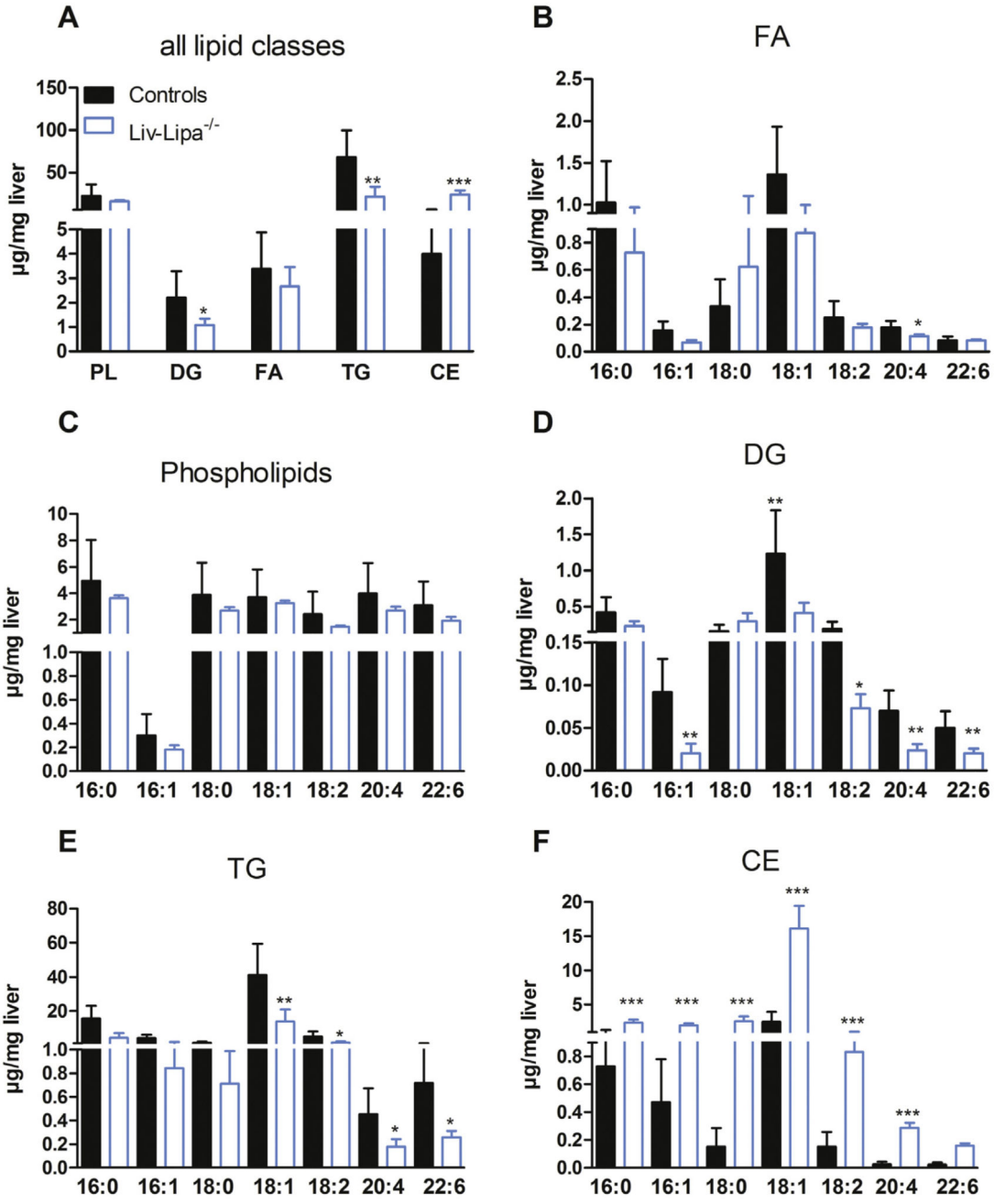

Fig. 6.

Accumulation of various FA species in hepatic CE fraction of HF/HCD-fed *Liv-Lipa*$^{-/-}$ mice. Female control and *Liv-Lipa*$^{-/-}$ mice were fed HF/HCD for 10 weeks. (A) GC analysis of hepatic lipid species after TLC separation. (B–F) GC analysis of FA composition for each major lipid class (FA-, PL-, DG-, TG-, and CE-corresponding bands after TLC separation). Data represent mean + SD; $p < 0.05$ (*), $p \leq 0.01$ (**), $p \leq 0.001$ (***) (n = 5–6). (A–F) Student's unpaired *t*-test.

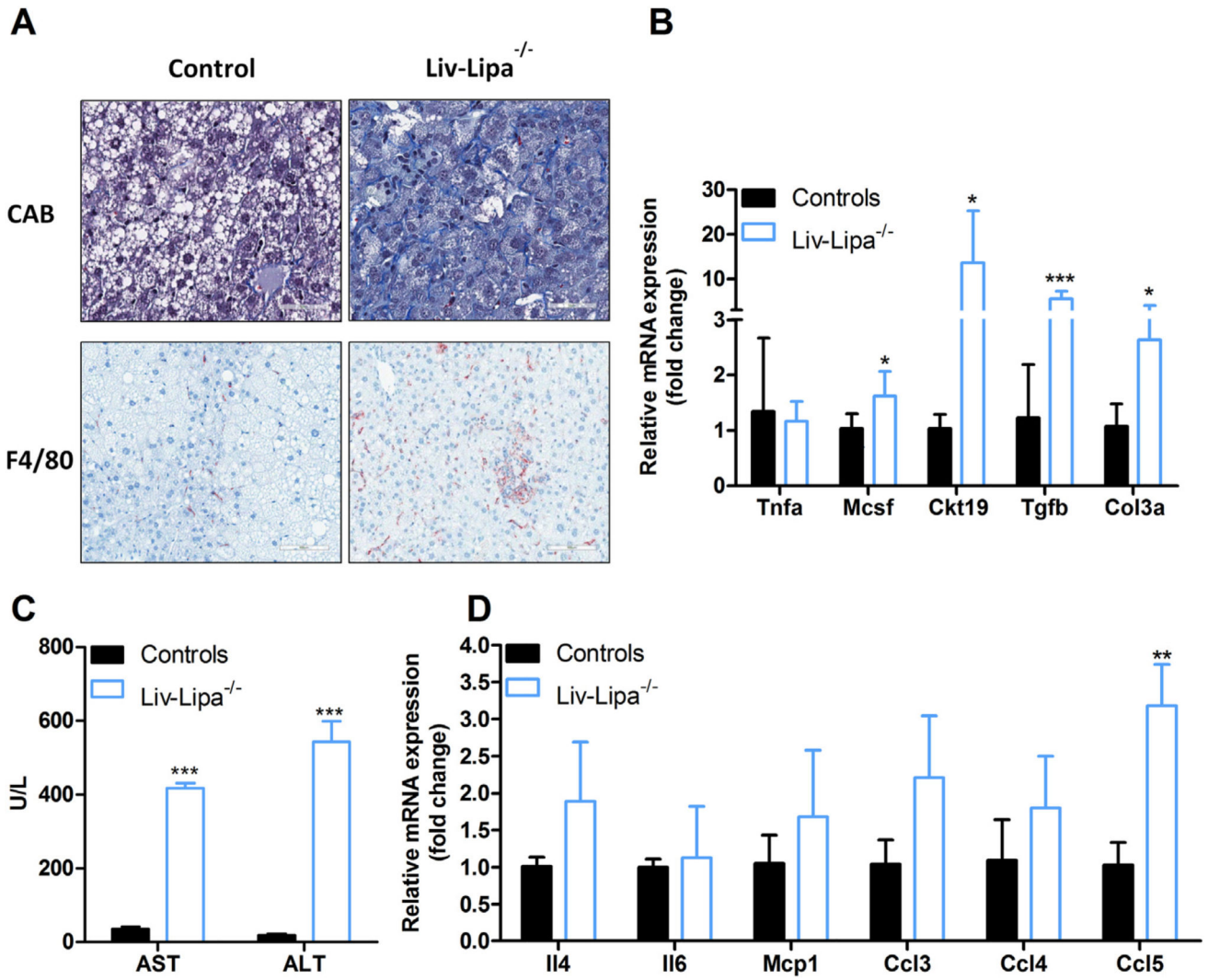

Fig. 7.

HF/HCD drives upregulation of cytokines, chemokines, and liver injury markers in *Liv-Lipa* $^{-/-}$ livers. (A) Liver sections of 20 week HF/HCD-fed male control and *Liv-Lipa*$^{-/-}$ mice stained with chromotrope aniline blue (CAB) as fibrosis marker (scale bar, 50 μm) and F4/80 as macrophage marker (scale bar, 100 μm). (B, D) Hepatic mRNA expression levels of liver injury markers, chemokines, and cytokines relative to cyclophilin A as reference gene in female mice fed HF/HCD for 20 weeks (n = 5–7). (C) Plasma concentrations of aspartate-aminotransferase (AST) and alanine aminotransferase (ALT) in female mice fed HF/HCD for 10 weeks (n = 3–4). Data represent mean values + SD; *p < 0.05, **p ≤ 0.01, ***p ≤ 0.001.